Tuning the Néel Temperature of Hexagonal Ferrites by Structural Distortion

Kishan Sinha,[1] Haohan Wang,[1] Xiao Wang,[2] Liying Zhou,[3,4] Yuewei Yin,[1] Wenbin Wang,[5] Xuemei Cheng,[2] David J. Keavney,[6] Huibo Cao,[7] Yaohua Liu,[7] Xifan Wu,[3] and Xiaoshan Xu[1,8]

[1]*Department of Physics and Astronomy, University of Nebraska, Lincoln, Nebraska 68588, USA*
[2]*Department of Physics, Bryn Mawr College, Bryn Mawr, Pennsylvania 19010, USA*
[3]*Department of Physics, Temple University, Philadelphia, Pennsylvania 19122, USA*
[4]*International Center for Quantum Materials, School of Physics, Peking University, Beijing 100871, Peoples Republic of China*
[5]*Department of Physics, Fudan University, Shanghai 200433, Peoples Republic of China*
[6]*Advanced Photon Source, Argonne National Laboratory, Argonne, Illinois 60439, USA*
[7]*Neutron Scattering Division, Oak Ridge National Lab, Oak Ridge, Tennessee 37831, USA*
[8]*Nebraska Center for Materials and Nanoscience, University of Nebraska, Lincoln, Nebraska 68588, USA*

(Received 9 July 2018; revised manuscript received 8 October 2018; published 7 December 2018)

To tune the magnetic properties of hexagonal ferrites, a family of magnetoelectric multiferroic materials, by atomic-scale structural engineering, we studied the effect of structural distortion on the magnetic ordering temperature (T_N) in these materials. Using the symmetry analysis, we show that unlike most antiferromagnetic rare-earth transition-metal perovskites, a larger structural distortion leads to a higher T_N in hexagonal ferrites and manganites, because the K_3 structural distortion induces the three-dimensional magnetic ordering, which is forbidden in the undistorted structure by symmetry. We also revealed a near-linear relation between T_N and the tolerance factor and a power-law relation between T_N and the K_3 distortion amplitude. Following the analysis, a record-high T_N (185 K) among hexagonal ferrites was predicted in hexagonal $ScFeO_3$ and experimentally verified in epitaxially stabilized films. These results add to the paradigm of spin-lattice coupling in antiferromagnetic oxides and suggests further tunability of hexagonal ferrites if more lattice distortion can be achieved.

DOI: 10.1103/PhysRevLett.121.237203

Spin-lattice couplings have a significant impact on magnetic properties. In antiferromagnetic (AFM) orthorhombic $RTMO_3$ (o-$RTMO_3$) for example, where R stands for rare earth, Y, or Sc, and TM stands for transition metal, a larger orthorhombic distortion from the cubic perovskite structure correlates with a lower Néel temperature (T_N), which may be understood as the reduction of the AFM superexchange interactions caused by the smaller TM-O-TM bond angles due to the orthorhombic distortions [1,2].

The effect of spin-lattice couplings may be employed to tune the magnetic properties. Here we focus on increasing the T_N of hexagonal $RFeO_3$, a family of multiferroics materials that are promising candidates for applications because of their spontaneous electric and magnetic polarizations, and potential magnetoelectric effects due to the coupling between the ferroelectric and the magnetic orders [3,4]. For widespread applications, it is important to increase the T_N of h-$RFeO_3$ [5], by, e.g., atomic-scale structural engineering based on the spin-lattice couplings.

On the other hand, in h-$RFeO_3$, T_N increases with the lattice distortion, which is a puzzling trend opposite to that in the AFM o-$RTMO_3$[see Fig. S1] [6]. Previously, Disseler *et al.* discovered a correlation between T_N and lattice constants in h-$RMnO_3$ and h-$RFeO_3$ [26]. The higher T_N for smaller R has been attributed to closer Fe-Fe (or Mn-Mn) distances [26,27]. This understanding is worth revisiting, since it cannot explain that in AFM o-$RTMO_3$, the smaller lattice constants do bring the TM atoms closer, but the reduced TM-O-TM bond angles actually decrease the AFM exchange interactions and T_N. Hence, there should be a distinct mechanism of magnetic ordering and spin-lattice coupling in h-$RMnO_3$ and h-$RFeO_3$. Elucidating this mechanism will not only provide guidance in increasing T_N of h-$RFeO_3$, but also add to the paradigms of spin-lattice coupling in AFM oxides.

In this work, we examine the role of the structural distortion in the magnetic ordering in h-$RMnO_3$ and h-$RFeO_3$. A symmetry analysis shows that the three-dimensional magnetic ordering is forbidden in the undistorted structure by symmetry, but can be induced by the K_3 distortion with a power-law relation between T_N and K_3 magnitude. Based on these revelations, we have predicted a record-high T_N in h-$RFeO_3$ when R = Sc and experimentally confirmed it in epitaxially stabilized films.

Hexagonal $ScFeO_3$ (001) and $YbFeO_3$ (001) films (5×5 mm^2 and 10×10 mm^2 surface area, 70–200 nm thick) have been grown on Al_2O_3 (001) and yttrium stabilized zirconia (YSZ) (111) respectively using pulsed laser (248 nm) deposition in a 5 mTorr oxygen environment, at 750 °C with a laser fluence of about 1.5 J/cm^2 and

a repetition rate of 2 Hz [28]. The film growth was monitored using the reflection high-energy electron diffraction (RHEED). The structural and magnetic properties have been studied using x-ray diffraction and spectroscopy, magnetometry, and neutron diffraction. X-ray diffraction experiments, including $\theta/2\theta$ scan, ϕ scan, and reciprocal space mapping were carried out using a Rigaku D/Max-B diffractometer with Co-$K\alpha$ radiation (1.793 Å wavelength) and a Rigaku SmartLab diffractometer with Cu-K radiation (1.5406 Å). X-ray absorption spectroscopy (including x-ray linear dichroism) with a 20° incident angle was studied at beam line 4-ID-C at the Advanced Photon Source at Argonne National Laboratory. Neutron diffraction experiments were carried out at beam line CORELLI at the Spallation Neutron Source (SNS) and HB3A four-circle diffractometer (FCD) at the High Flux Reactor (HFIR) with a thermal neutron wavelength of 1.546 Å, in the Oak Ridge National Laboratory. Temperature and magnetic-field dependence of the magnetization was measured using a superconducting quantum interference device (SQUID) magnetometer with the field along the film normal direction.

The crystal structure of isomorphic hexagonal $R\mathrm{MnO_3}$ and $R\mathrm{FeO_3}$ (h-$R\mathrm{MnO_3}$ and h-$R\mathrm{FeO_3}$) has a $P6_3\mathrm{cm}$ symmetry, consisting of alternating FeO (or MnO) and RO_2 layers [Fig. 1(a)]. AFM orders occur in h-$R\mathrm{MnO_3}$ and h-$R\mathrm{FeO_3}$ below about 70–140 K with spins in the FeO (or MnO) layers forming 120° structures [26,29–32]. Below about 1000 K, ferroelectricity in h-$R\mathrm{MnO_3}$ and h-$R\mathrm{FeO_3}$ is induced by a lattice distortion (K_3) [Fig. 1(a)] which tilts the $\mathrm{FeO_5}$ (or $\mathrm{MnO_5}$) local environment, shifts the R atoms along the c axis, and trimerizes the unit cell, with a sizable electric polarization ($P \approx 10\ \mu\mathrm{C/cm^2}$) [33–36]. In addition, hexagonal $R\mathrm{FeO_3}$ exhibits a weak ferromagnetism [26,30,34,35,37,38] [Fig. 1(a)] due to the canting Fe spins.

Magnetic ordering relies on the underlying exchange interactions. In h-$R\mathrm{FeO_3}$ and h-$R\mathrm{MnO_3}$, although the exchange interactions within the FeO (or MnO) layers are strong, the interlayer exchange interactions are weakened by the layered structure and hexagonal stacking. Using h-$R\mathrm{FeO_3}$ as an example, Fig. 1(b) shows the arrangement of the Fe atoms and their spins in two neighboring FeO layers. The Fe atoms are on the hexagonal A and C sites in the two layers, respectively. One Fe atom ($\mathrm{Fe_0}$) in the $z = c/2$ layer is highlighted by its tilted $\mathrm{FeO_5}$ trigonal bipyramid. The interlayer nearest-neighbor exchange energy for $\mathrm{Fe_0}$ is $E_{\mathrm{inter}} = \sum_{i=1}^{3} J_{0i}\vec{S}_0 \cdot \vec{S}_i$, where S_i is the spin on Fe_i, and J_{0i} is the exchange interaction coefficient between $\mathrm{Fe_0}$ and Fe_i. When there is no lattice distortion, the local symmetry of $\mathrm{Fe_0}$ is C_{3v}, leading to $J_{01} = J_{02} = J_{03}$ and $E_{\mathrm{inter}} = 0$ because $\sum_{i=1}^{3} \vec{S}_i = 0$. In other words, the interlayer exchange interactions are canceled; the spin alignment between the two layers is lost. Therefore, the three-dimensional magnetic ordering is forbidden in the undistorted $P6_3/\mathrm{mmc}$ structure by symmetry.

On the other hand, the K_3 lattice distortion [Fig. 1(a)] reduces the symmetry to C_S, making $J_{03} \neq J_{02} = J_{01}$. Consequently, nonzero lattice distortion leads to the three-dimensional magnetic ordering because $E_{\mathrm{inter}} = (J_{01}\text{–}J_{03})S(S+1) \neq 0$ [39]. Since the interlayer exchange interaction is the bottleneck of the three-dimensional magnetic ordering, one has $T_N \propto E_{\mathrm{inter}} = (J_{01}\text{–}J_{03})S(S+1)$. The dependence of T_N on the K_3 distortion then hinges on the relation between $J_{01}\text{–}J_{03}$ and the magnitude of K_3 (Q_{K3}). Previously, Das *et al.* analyzed the relation between $J_{01}\text{–}J_{03}$ and Q_{K3} [3]. Expanding J_{01} and J_{03} with respect to Q_{K3} around $Q_{K3} = 0$, the odd terms are expected to be zero due to the symmetry at $Q_{K3} = 0$, leaving $J_{01}\text{–}J_{03} \propto a_2 Q_{K3}^2 + a_4 Q_{K3}^4$, where a_2 and a_4 are coefficients. In Fig. 1(c), we plot the $\log\{T_N/[S(S+1)]\}$ as a

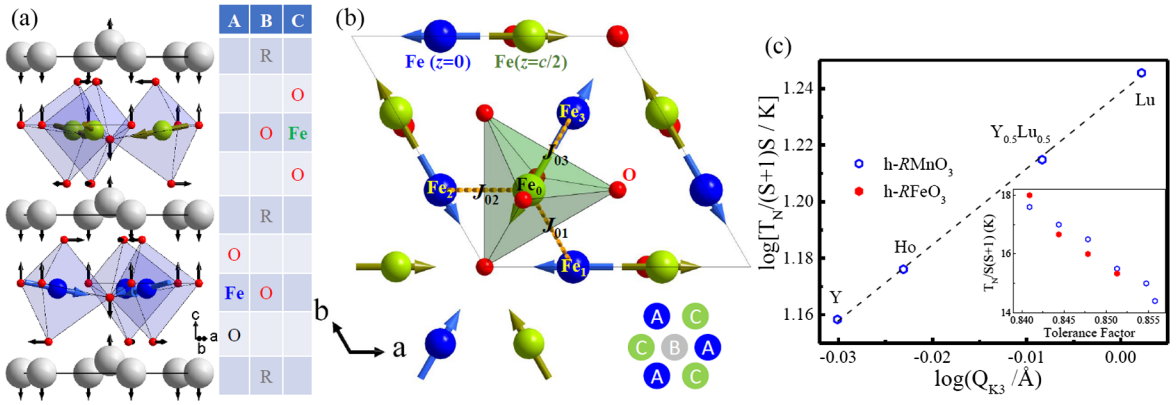

FIG. 1. (a) Atomic structure of h-$R\mathrm{FeO_3}$ depicted by a hexagonal unit cell. The arrows through the Fe atoms indicate the spins. The arrows from the atoms indicate the atomic displacements of the K_3 lattice distortion. The table indicates the hexagonal stacking. (b) The geometric arrangement of Fe atoms in the $z = 0$ and $z = c/2$ layers. The arrows through the Fe atoms indicate the spins. The atom $\mathrm{Fe_0}$ is highlighted by its $\mathrm{FeO_5}$ trigonal bipyramid to depict the local symmetry. (c) $\log\{T_N/[S(S+1)]/K\}$ as a function of $\log(Q_{K_3})$. Inset: $T_N/[S(S+1)]$ as a function of the tolerance factor. The dashed line is a linear fit to the data. The data are from the literature (see text).

function of $\log(Q_{K3})$ of h-RMnO$_3$ measured using the neutron diffraction from the literature [40,41] [see Fig. S2] [6], where spin S is 2 for Mn. The data appear to fall on a straight line, indicating a power-law relation $T_N/[S(S+1)] \propto Q_{K_3}^n$; a fit shows $n = 2.7 \pm 0.05$. Given that the tilt of FeO$_5$ and MnO$_5$ caused by the K_3 distortion is on the order of several degrees which is not so small [29,40,41], both the $a_2 Q_{K3}^2$ and the $a_4 Q_{K3}^4$ terms could play a role, resulting $2 < n < 4$.

It is challenging to predict the T_N using the direct dependence of T_N on the K_3 distortion, however, because the K_3 distortion, which involves the displacement of oxygen atoms, is difficult to measure precisely. The tolerance factor $t = (r_R + r_O)/[(r_{TM} + r_O)\sqrt{2}]$ where r_R, r_{TM}, and r_O are atomic radius of R, TM and oxygen, is a good measure of lattice distortion from the cubic perovskite structure in o-RTMO$_3$. It could also be used to gauge the structural distortion in h-RFeO$_3$ and h-RMnO$_3$, because a smaller R atom is expected to reduce the in-plane lattice constant, which needs to be accommodated by a larger K_3 distortion to reduce the distances between Fe (or Mn) atoms within the FeO (or MnO) layers. In other words, smaller t is expected to lead to larger T_N, which is consistent with the data from the literature [Fig. 1(c) inset and Fig. S2] [6,31,40,41], where a linear correlation between $T_N/[S(S+1)]$ and t in h-RFeO$_3$ and h-RMnO$_3$ is observed (S is 2 and 2.5 for Mn and Fe, respectively).

Following the trend in Fig. 1(c), a smaller R, corresponding to a smaller t, will lead to a higher T_N in h-RFeO$_3$ and h-RMnO$_3$. Since Sc has a much smaller atomic radius than that of the rare earth and Y [42], T_N in h-ScFeO$_3$ is expected to be higher than that of other h-RFeO$_3$. To verify the prediction, we studied the magnetic ordering temperature in h-ScFeO$_3$. ScFeO$_3$ naturally crystallizes in bixbyite structure in bulk; high pressure growth of ScFeO$_3$ results in a corundum structure [43]. Previous studies show that partially substituting Lu with Sc in LuFeO$_3$ may stabilize the hexagonal structure [26,27,44]. However, the stabilization of pure ScFeO$_3$ in the $P6_3$cm structure has never been reported. In this study, we have successfully grown h-ScFeO$_3$ epitaxial films on Al$_2$O$_3$ (001) substrates. The crystal structure and epitaxial relations of the h-ScFeO$_3$ films were characterized using x-ray diffraction. As shown in Fig. 2(a), the $\theta/2\theta$ scan shows a typical pattern of the $P6_3$cm structure with the epitaxial relation: h-ScFeO$_3$ (001) $\parallel$ Al$_2$O$_3$ (001). The ϕ scan [see Fig. S3] [6] demonstrates the sixfold rotation symmetry and the in-plane epitaxial relation: h-ScFeO$_3$ (100) $\parallel$ Al$_2$O$_3$ (100). The RHEED patterns [Figs. 2(b) and 2(c)], which are signatures of the h-RFeO$_3$ structure, indicate a flat surface. The FeO$_5$ trigonal bipyramid configuration is confirmed by the similarity between the x-ray linear dichroism spectroscopy of h-ScFeO$_3$ [Fig. 2(d)] and those of h-LuFeO$_3$ and h-YbFeO$_3$ observed previously [28,45–47]. From the x-ray reciprocal space mapping [see Fig. S3] [6], the lattice

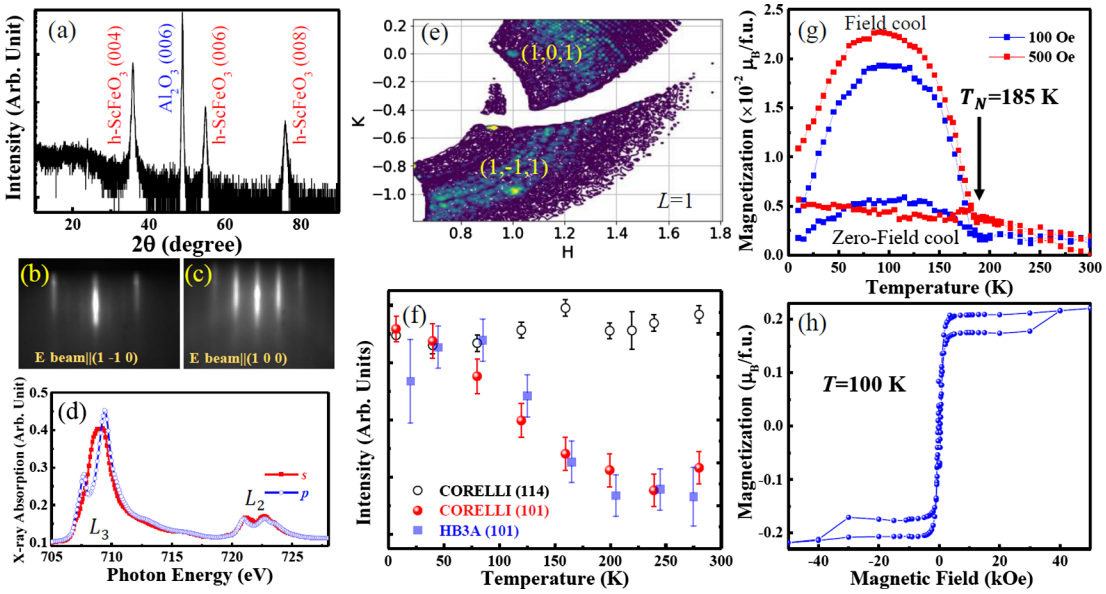

FIG. 2. Structural and magnetic characterizations of h-ScFeO$_3$(001)/Al$_2$O$_3$ films. (a) $\theta/2\theta$ x-ray (1.789 Å) diffraction. (b) and (c) are the RHEED diffraction patterns measured when the electron beam are along the (1-10) and (100) directions respectively. (d) X-ray absorption spectra measured at the Fe L edges using s (in plane) and p (out of plane) linearly polarized x-ray beams. (e) A slice of the reciprocal space of h-ScFeO$_3$ at $L = 1$ measured using neutron diffraction at CORELLI (see text). (f) Temperature dependence of the neutron diffraction intensities of the (101) and (114) peaks measured at CORELLI and HB3A. (g) Temperature dependence of the magnetization per formula unit (f.u.) measured during warming after field cool (10 kOe) and zero field cool using 100 Oe and 500 Oe. (h) Magnetization-field hysteresis loop measured at 100 K. The magnetic field is along the film normal direction.

constants of h-$ScFeO_3$ were determined: $a = 5.742$ Å and $c = 11.690$ Å, smaller than the values of other h-$RFeO_3$ [48–50], suggesting a larger lattice distortion [51].

T_N of h-$ScFeO_3$ was measured by the neutron diffraction experiments at CORELLI in addition to that of h-$YbFeO_3$. Using a wide wave-length-band neutron beam and a two-dimensional detector at CORELLI, a three-dimensional portion of the reciprocal space [using the Miller indices (H, K, L) as the coordinates] can be measured without rotating the sample [see Figs. S4–S7] [6]. The (101) and (114) diffraction peaks, were mapped out in the three-dimensional reciprocal space. As shown in Fig. 2(e), the two magnetic Bragg diffraction peaks (101) and (1-11), which are equivalent because of the sixfold rotational symmetry along the c axis, were observed. The (101) Bragg peak is forbidden for the nuclear diffraction due to the crystal structure symmetry of h-$RFeO_3$ (space group $P6_3cm$), but it is allowed for magnetic diffraction [29]. The observation of the (101) peak confirms the magnetic ordering in h-$RFeO_3$, as previously shown in h-$LuFeO_3$ and h-$RMnO_3$ [26,29,32]. The temperature dependence of the (101) peak intensity suggests a transition at about 200 K, which is corroborated by the measurements at HB3A [Fig. 2(f)]. In contrast, the intensity of the (114) peak, which mainly comes from the nuclear scattering, shows an insignificant temperature dependence. As shown in Fig. 2(g), a similar transition temperature is observed in the temperature dependence of the magnetization measured using a SQUID magnetometer on warming, after cooling the sample in a 10 kOe magnetic field (field cool or FC) and after cooling in a zero magnetic field (zero-field cool or ZFC). The FC and ZFC curves diverge at around 185 K, giving a more precise determination of T_N.

As predicted, h-$ScFeO_3$ shows a high T_N among all h-$RMnO_3$ and h-$RFeO_3$, as shown in Fig. 3(a), where our measurement on h-$YbFeO_3$ and data in the literature are also included [See Figs. S3 and S4] [6,26,29,31–35,37,41]; the measured T_N of h-$ScFeO_3$ is slightly lower than the value predicted by extrapolating the linear relation between T_N and t, which is also true for h-$ScMnO_3$ [29]. The reduction of magnetization at low temperature in Fig. 2(g) hints at a possible spin reorientation at about 100 K in h-$ScFeO_3$. However, the temperature dependence of the (101) peak intensity in Fig. 2(f) indicates that spin reorientation in h-$ScFeO_3$ may not be significant enough to change the spin structure from A_2 to A_1 [26].

Finally, we discuss the effect of lattice distortion on the canting of Fe moments, which is responsible for the net magnetization M_{Fe} along the c axis. The M_{Fe} in h-$ScFeO_3$ can be inferred from the magnetometry data. As shown in Fig. 2(h), the M–H curve shows a soft and a hard component, corresponding to two steps at $H \approx 0$ and $H \approx 30$ kOe, respectively. This two-component feature has been observed in both h-$LuFeO_3$ and h-$YbFeO_3$ films [38,45]. The jump of magnetization at the higher field corresponds to the intrinsic coercivity of the h-$RFeO_3$, while the jump at the low field corresponds to the unavoidable structural boundaries in film samples of h-$RFeO_3$ that create uncompensated spins. From the 30-kOe jump, we found that $M_{Fe} = 0.015 \pm 0.002$ μ_B/Fe in h-$ScFeO_3$, which is smaller than that of h-$LuFeO_3$ and h-$YbFeO_3$ [38,45], as shown in Fig. 3(b). This result is counterintuitive, because a large K_3 distortion, corresponding to a larger tilt angle of the FeO_5 would seemingly generate a larger canting angle of the Fe moments (θ_{cant}). However, θ_{cant} results from a competition between the exchange interaction and the Dzyaloshinskii-Moriya (DM) interaction [52–54]. Relation between the canting angle (θ_{cant}) of the Fe moments, tilt angle of the FeO_5 (γ_{tilt}), lattice constant in the basal plane (a), and the intralayer exchange interaction coefficient J can be derived as $\theta_{cant} \propto a^2\gamma_{tilt}/J$ [See Fig. S8] [6]. Although h-$ScFeO_3$ is expected to have a larger γ_{tilt} and smaller J, a is also smaller. Hence, the size of θ_{cant} cannot be simply linked to the amplitude of γ_{tilt}. If the effect of a dominates, M_{Fe} would decrease for smaller R, which is what we found in our previous first-principle calculations [51].

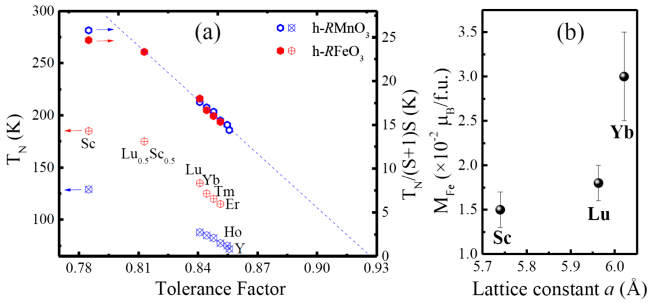

FIG. 3. (a) The dependence of T_N and $T_N/S(S+1)$ on the tolerance factor. The dashed line is a guide to the eye. (b) The magnetization from the canting of Fe spins (M_{Fe}) as a function of the in-plane lattice constant. Except for h-$YbFeO_3$ and h-$ScFeO_3$ in (a) and h-$ScFeO_3$ in (b), the data are from the literature (see text).

In conclusion, using symmetry analysis, we showed that the three-dimensional magnetic ordering in h-$RMnO_3$ and h-$RFeO_3$ are forbidden in undistorted structures by symmetry, but can be induced by the structural distortions. We also showed that the dependence of T_N on structural distortions manifests as a near-linear relation with the tolerance factor and a possible power law with Q_{K3}, suggesting a higher T_N in h-$ScFeO_3$ with respect to other hexagonal ferrites studied so far, which was realized in this work in epitaxially stabilized films. In addition to indicating that the multiferroic ordering in h-$RFeO_3$ and h-$RMnO_3$ may be further enhanced with larger lattice distortions, these results also establish a paradigm of structural origin of magnetic ordering and spin-lattice coupling in AFM oxides.

This work was primarily supported by the National Science Foundation (NSF), Division of Materials Research (DMR) under Grant No. DMR-1454618. X. W. was supported by National Science Foundation through Grant No. DMR-1552287. X. M. C. acknowledges partial support from NSF DMR-1708790 and DMR-1053854. This research used resources at the Spallation Neutron Source and the High Flux Isotope Reactor, DOE Office of Science User Facilities operated by the Oak Ridge National Laboratory, and resources of the Advanced Photon Source, a U.S. Department of Energy (DOE) Office of Science User Facility operated for the DOE Office of Science by Argonne National Laboratory under Contract No. DE-AC02-06CH11357. The research was performed in part in the Nebraska Nanoscale Facility: National Nanotechnology Coordinated Infrastructure and the Nebraska Center for Materials and Nanoscience, which are supported by the National Science Foundation under Grant No. ECCS-1542182, and the Nebraska Research Initiative.

[1] J. B. Goodenough, J. Phys. Chem. Solids **6**, 287 (1958).
[2] J. Kanamori, J. Phys. Chem. Solids **10**, 87 (1959).
[3] H. Das, A. L. Wysocki, Y. Geng, W. Wu, and C. J. Fennie, Nat. Commun. **5**, 2998 (2014).
[4] M. Ye and D. Vanderbilt, Phys. Rev. B **92**, 035107 (2015).
[5] J. A. Mundy *et al.*, Nature (London) **537**, 523 (2016).
[6] See Supplemental Material at http://link.aps.org/supplemental/10.1103/PhysRevLett.121.237203 for more information on the survey of literature about the relation between T_N and structural distortion, x-ray and neutron diffraction, and the discussion about Fe moment canting, which includes additional Refs. [7–25].
[7] A. S. Bhalla, R. Guo, and R. Roy, Mater. Res. Innovations **4**, 3 (2000).
[8] H. D. Zhou and J. B. Goodenough, J. Phys. Condens. Matter **17**, 7395 (2005).
[9] E. F. Bertaut, G. Bassi, G. Buisson, P. Burlet, J. Chappert, A. Delapalme, J. Mareschal, G. Roult, R. Aleonard, R. Pauthenet, and J. P. Rebouillat, J. Appl. Phys. **37**, 1038 (1966).
[10] T. Sakai, G. Y. Adachi, J. Shiokawa, and T. Shin-Ike, J. Appl. Phys. **48**, 379 (1977).
[11] A. Munoz, J. A. Alonso, M. T. Casais, M. J. Martinez-Lope, J. L. Martinez, and M. T. Fernandez-Diaz, Phys. Rev. B **68**, 144429 (2003).
[12] M. Reehuis, C. Ulrich, P. Pattison, B. Ouladdiaf, M. C. Rheinstadter, M. Ohl, L. P. Regnault, M. Miyasaka, Y. Tokura, and B. Keimer, Phys. Rev. B **73**, 094440 (2006).
[13] M. Reehuis, C. Ulrich, K. Prokes, S. Matas, J. Fujioka, S. Miyasaka, Y. Tokura, and B. Keimer, Phys. Rev. B **83**, 064404 (2011).
[14] C. Ritter, S. A. Ivanov, G. V. Bazuev, and F. Fauth, Phys. Rev. B **93**, 054423 (2016).
[15] F. Moussa, M. Hennion, J. Rodriguez-Carvajal, H. Moudden, L. Pinsard, and A. Revcolevschi, Phys. Rev. B **54**, 15149 (1996).
[16] Z. Jirak, J. Hejtmanek, E. Pollert, M. Marysko, M. Dlouha, and S. Vratislav, J. Appl. Phys. **81**, 5790 (1997).
[17] A. Muoz, J. A. Alonso, M. J. Martnez-Lope, J. L. Garca-Muoz, and M. T. Fernndez-Daz, J. Phys. Condens. Matter **12**, 1361 (2000).
[18] J. G. Cheng, J. S. Zhou, J. B. Goodenough, Y. T. Su, Y. Sui, and Y. Ren, Phys. Rev. B **84**, 104415 (2011).
[19] T. Kimura, G. Lawes, T. Goto, Y. Tokura, and A. P. Ramirez, Phys. Rev. B **71**, 224425 (2005).
[20] M. L. Medarde, J. Phys. Condens. Matter **9**, 1679 (1997).
[21] J. A. Alonso, M. J. Martnez-Lope, M. T. Casais, J. L. Martnez, G. Demazeau, A. Largeteau, J. L. Garca-Muoz, A. Muoz, and M. T. Fernndez-Daz, Chem. Mater. **11**, 2463 (1999).
[22] M. T. Fernández-Díaz, J. A. Alonso, M. J. Martinez-Lope, M. T. Casais, and J. L. García-Muñoz, Phys. Rev. B **64**, 144417 (2001).
[23] H. Tan, C. Xu, M. Li, S. Wang, B. L. Gu, and W. Duan, J. Phys. Condens. Matter **28**, 126002 (2016).
[24] C. Xu, Y. Yang, S. Wang, W. Duan, B. Gu, and L. Bellaiche, Phys. Rev. B **89**, 205122 (2014).
[25] B. D. Cullity, *Elements of X-Ray Diffraction* (Addison-Wesley, Reading, MA, 1956).
[26] S. M. Disseler, X. Luo, B. Gao, Y. S. Oh, R. Hu, Y. Wang, D. Quintana, A. Zhang, Q. Huang, J. Lau, R. Paul, J. W. Lynn, S. W. Cheong, and W. Ratcliff, Phys. Rev. B **92**, 054435 (2015).
[27] A. Masuno, A. Ishimoto, C. Moriyoshi, N. Hayashi, H. Kawaji, Y. Kuroiwa, and H. Inoue, Inorg. Chem. **52**, 11889 (2013).
[28] S. Cao, X. Zhang, T. R. Paudel, K. Sinha, X. Wang, X. Jiang, W. Wang, S. Brutsche, J. Wang, P. J. Ryan, J.-W. Kim, X. Cheng, E. Y. Tsymbal, P. A. Dowben, and X. Xu, J. Phys. Condens. Matter **28**, 156001 (2016).
[29] A. Munoz, J. A. Alonso, M. J. Martinez-Lope, M. T. Casais, J. L. Martinez, and M. T. Fernandez-Diaz, Phys. Rev. B **62**, 9498 (2000).
[30] W. Wang, J. Zhao, W. Wang, Z. Gai, N. Balke, M. Chi, H. N. Lee, W. Tian, L. Zhu, X. Cheng, D. J. Keavney, J. Yi, T. Z. Ward, P. C. Snijders, H. M. Christen, W. Wu, J. Shen, and X. Xu, Phys. Rev. Lett. **110**, 237601 (2013).
[31] M. Fiebig, T. Lottermoser, and R. V. Pisarev, J. Appl. Phys. **93**, 8194 (2003).
[32] S. M. Disseler, J. A. Borchers, C. M. Brooks, J. A. Mundy, J. A. Moyer, D. A. Hillsberry, E. L. Thies, D. A. Tenne, J. Heron, M. E. Holtz, J. D. Clarkson, G. M. Stiehl, P. Schiffer, D. A. Muller, D. G. Schlom, and W. D. Ratcliff, Phys. Rev. Lett. **114**, 217602 (2015).
[33] Y. K. Jeong, J. Lee, S. Ahn, and H. M. Jang, Chem. Mater. **24**, 2426 (2012).
[34] Y. K. Jeong, J. Lee, S. Ahn, S.-W. Song, H. M. Jang, H. Choi, and J. F. Scott, J. Am. Chem. Soc. **134**, 1450 (2012).
[35] S.-J. Ahn, J.-H. Lee, H. M. Jang, and Y. K. Jeong, J. Mater. Chem. C **2**, 4521 (2014).
[36] P. Murugavel, J. H. Lee, D. Lee, T. W. Noh, Y. Jo, M. H. Jung, Y. S. Oh, and K. H. Kim, Appl. Phys. Lett. **90**, 142902 (2007).

[37] H. Yokota, T. Nozue, S. Nakamura, H. Hojo, M. Fukunaga, P. E. Janolin, J. M. Kiat, and A. Fuwa, Phys. Rev. B **92**, 054101 (2015).
[38] J. A. Moyer, R. Misra, J. A. Mundy, C. M. Brooks, J. T. Heron, D. A. Muller, D. G. Schlom, and P. Schiffer, APL Mater. **2**, 012106 (2014).
[39] H. Wang, I. V. Solovyev, W. Wang, X. Wang, P. J. Ryan, D. J. Keavney, J.-W. Kim, T. Z. Ward, L. Zhu, J. Shen, X. M. Cheng, L. He, X. Xu, and X. Wu, Phys. Rev. B **90**, 014436 (2014).
[40] S. Lee, A. Pirogov, M. Kang, K.-H. Jang, M. Yonemura, T. Kamiyama, S.-W. Cheong, F. Gozzo, N. Shin, H. Kimura, Y. Noda, and J.-G. Park, Nature (London) **451**, 805 (2008).
[41] A. Munoz, J. Alonso, M. Martinez-Lopez, M. Cesais, J. Martinez, and M. Fernandez-Diaz, Chem. Mater. **13**, 1497 (2001).
[42] R. D. Shannon, Acta Crystallogr. Sect. A **32**, 751 (1976).
[43] M. Li, U. Adem, S. R. C. Mcmitchell, Z. Xu, C. I. Thomas, J. E. Warren, D. V Giap, H. Niu, X. Wan, R. G. Palgrave, F. Schiffmann, F. Cora, B. Slater, T. L. Burnett, M. G. Cain, A. M. Abakumov, G. Van Tendeloo, M. F. Thomas, M. J. Rosseinsky, and J. B. Claridge, J. Am. Chem. Soc. **134**, 3737 (2012).
[44] L. Lin, H. M. Zhang, M. F. Liu, S. Shen, S. Zhou, D. Li, X. Wang, Z. B. Yan, Z. D. Zhang, J. Zhao, S. Dong, and J.-M. Liu, Phys. Rev. B **93**, 075146 (2016).
[45] S. Cao, K. Sinha, X. Zhang, X. Zhang, X. Wang, Y. Yin, A. T. NDiaye, J. Wang, D. J. Keavney, T. R. Paudel, Y. Liu, X. Cheng, E. Y. Tsymbal, P. A. Dowben, and X. Xu, Phys. Rev. B **95**, 224428 (2017).
[46] S. Cao, X. Zhang, K. Sinha, W. Wang, J. Wang, P. A. Dowben, and X. Xu, Appl. Phys. Lett. **108**, 202903 (2016).
[47] W. Wang, H. Wang, X. Xu, L. Zhu, L. He, E. Wills, X. Cheng, D. J. Keavney, J. Shen, X. Wu, and X. Xu, Appl. Phys. Lett. **101**, 241907 (2012).
[48] X. Zhang, Y. Yin, S. Yang, Z. Yang, and X. Xu, J. Phys. Condens. Matter **29**, 164001 (2017).
[49] E. Magome, C. Moriyoshi, Y. Kuroiwa, A. Masuno, and H. Inoue, Jpn. J. Appl. Phys. **49**, 09ME06 (2010).
[50] A. A. Bossak, I. E. Graboy, O. Y. Gorbenko, A. R. Kaul, M. S. Kartavtseva, V. L. Svetchnikov, and H. W. Zandbergen, Chem. Mater. **16**, 1751 (2004).
[51] K. Sinha, Y. Zhang, X. Jiang, H. Wang, X. Wang, X. Zhang, P. J. Ryan, J.-W. Kim, J. Bowlan, D. A. Yarotski, Y. Li, A. D. DiChiara, X. Cheng, X. Wu, and X. Xu, Phys. Rev. B **95**, 094110 (2017).
[52] I. Dzyaloshinsky, J. Phys. Chem. Solids **4**, 241 (1958).
[53] T. Moriya, Phys. Rev. **120**, 91 (1960).
[54] F. Keffer, Phys. Rev. **126**, 896 (1962).